Dalton Transactions

PAPER

View Article Online
View Journal

Cite this: DOI: 10.1039/c6dt02878k

Cytotoxicity and biodistribution studies of luminescent Au(I) and Ag(I) N-heterocyclic carbenes. Searching for new biological targets†

Renso Visbal,[a,b] Vanesa Fernández-Moreira,[a] Isabel Marzo,[c] Antonio Laguna[a] and M. Concepción Gimeno*[a]

Received 20th July 2016,
Accepted 8th August 2016

DOI: 10.1039/c6dt02878k

www.rsc.org/dalton

A range of fluorescent and biologically compatible gold(I)–N-heterocyclic carbenes bearing acridine as a wingtip group and either a 2-mercaptopyridine or a tetra-*O*-acetyl-1-thio-β-D-glucopyranoside as an ancillary ligand has been synthesised. Their luminescence, cytotoxicity and biodistribution have been investigated together with those of analogous gold(I) and silver(I) chloride- and bis-NHC complexes. All complexes displayed emissions based on IL transitions centred on the acridine moiety. The cytotoxic activity measured in lung, A549, and pancreatic, MiaPaca2, carcinoma cell lines revealed a general cytotoxicity pattern (thiolate > biscarbene > chloride derivatives) and flow cytometry assays pointed towards apoptosis as the cell death mechanism. Moreover, fluorescence cell microscopy disclosed an unusual biodistribution behavior, being mainly localised in lysosomes and to a lesser extent in the nucleus. Preliminary DNA interaction experiments suggested the metal fragment and not the acridine moiety as responsible for such biodistribution, which widen the scope for new biological targets.

Introduction

Medicinal inorganic chemistry has offered many new opportunities for the design of therapeutic agents with excellent biological properties not exhibited by organic compounds.[1] Cisplatin has become a global benchmark in the use of metal based drugs for the treatment of a variety of tumors, in particular ovarian and testicular cancer.[2] Alternatively, gold chemistry is one of the most developed research areas for this purpose, and after the discovery of the great activity of auranofin against rheumatoid arthritis,[3] several Au(I) and Au(III) complexes have been described as potent antiarthritic, antitumor and antimalarial agents.[4] One of the major differences between the antitumor activity of cisplatin and gold compounds lies in their different biological targets. The first one normally acts by direct interaction with DNA,[2] whereas the antiproliferative activity of gold complexes is believed to affect the functionality of the mitochondria. Numerous studies point to the inhibition of the enzyme thioredoxin reductase (TrxR),[5] which is in charge of regenerating the functionality of small molecules as well as controlling the cellular redox homeostasis. Two isoforms are known for this enzyme, one located in the cytosol and the other situated in the mitochondria. In both cases, the TrxR is involved in the reduction of thioredoxin (Trx) to its dithiolic form, and the inhibition of this enzyme leads to apoptosis *via* a mitochondrial pathway.[6]

Within the same frame, silver complexes bearing phosphine ligands have been reported to inhibit the same TrxR enzyme.[7] Among the gold and silver derivatives studied lately, N-heterocyclic carbene (NHC) complexes are emerging as a promising class of metallodrugs.[8] Their particular stability and electronic properties make them versatile ligands capable of binding to a wide variety of metals with direct application in important research areas, *i.e.* catalysis,[9] photoactive materials,[10] liquid crystals,[11] metal–organic frameworks[12] and metallopharmaceuticals.[8,13] The strong σ-donating ability of NHCs is comparable to that of phosphines, and many research groups have been developing and evaluating Au(I), Au(III) and Ag(I)–NHC complexes as new anticancer agents.[14] Incorporation of an organic or organometallic chromophoric group within the carbene structure has become a straightforward

[a]*Departamento de Química Inorgánica, Instituto de Síntesis Química y Catálisis Homogénea, CSIC-Universidad de Zaragoza, Pedro Cerbuna 12, 50009 Zaragoza, Spain. E-mail: gimeno@unizar.es; Fax: +34 976761187; Tel: +34 976762291*
[b]*Programa de Ingeniería Industrial, Facultad de Ingeniería, Universidad de la Costa, Calle 58 # 55-66, 080001 Barranquilla, Colombia*
[c]*Departamento de Bioquímica y Biología Molecular, Universidad de Zaragoza, 50009 Zaragoza, Spain*

†Electronic supplementary information (ESI) available: X-ray crystallographic data bond angles and distances for complex **10** (Tables S1 and S2). Normalised emission spectra of complexes **10** and **1** (Fig. S1). Cytotoxicity assay of complexes **1–12** (Fig. S2). Additional images of A549 cells incubated with complexes **1**, **5**, **6**, **8**, **10**, **11** and **12** (Fig. S3–S5). CCDC 1471431 for complex **10**. For ESI and crystallographic data in CIF or other electronic format see DOI: 10.1039/c6dt02878k

strategy to be able to use modern confocal fluorescence microscopy techniques, which definitely would lead to the development of improved theranostic agents. Consequently, crucial information such as cellular uptake, biodistribution and/or bioaffinity would definitively be of vital importance for the elucidation of the structure–activity relationship.[15] Only a few examples of Au(I)–NHC and Ag(I)–NHC complexes with organic chromophores have been reported.[14b,16] Contrary to what was expected considering the great capacity of Au(I) and Ag(I) derivatives to inhibit the TrxR, most of them did not show mitochondrial localization, suggesting additional targets within the cells, Fig. 1.[14b,16] Therefore, it is extremely important to go in depth in search of new targets for gold and silver derivatives to know and tackle all the premises in the design of optimised metallodrugs.

In a previous work, we have reported some silver(I) and gold(I) complexes containing acridine-based NHC ligands (Fig. 2), which showed the characteristic optical properties assigned mainly to intraligand (IL) transitions centred on the acridine group.[17] This chromophore group is well known for being a DNA intercalator. Consequently, these gold and silver NHC complexes can have additional biological predisposition to interact with the DNA,[18] affording bifunctional probes.

With this idea in mind, and taking into account that complexes **1–8** showed optimal emissive properties in solution to be used as cell imaging agents, we aimed to further study their antiproliferative activity against different tumor cell lines, A-549 (lung carcinoma) and Mia-Paca2 (pancreatic carcinoma), as well as to elucidate the intracellular biodistribution by fluorescence microscopy. In order to evaluate the effects of the presence of bioactive molecules, additional thiolate acridine–NHC based Au(I) complexes containing thiopyridine or tetra-*O*-acetyl-1-thio-β-D-glucopyranoside fragments were chosen to be incorporated into the Au(I)–NHC motifs.

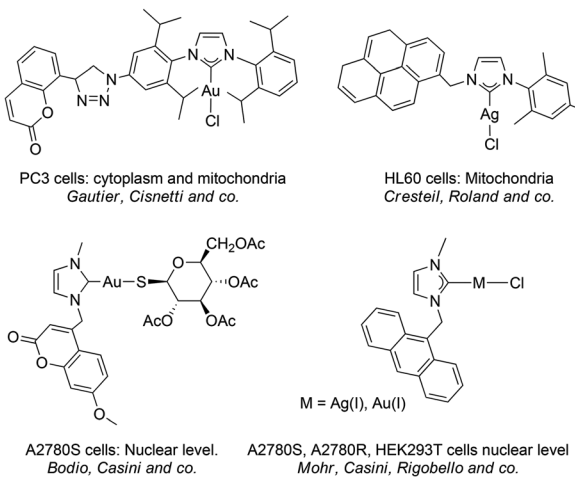

Fig. 1 N-Heterocyclic Ag(I) and Au(I) carbene complexes with their correspondent biodistribution using fluorescence confocal microscopy techniques.[14b,16].

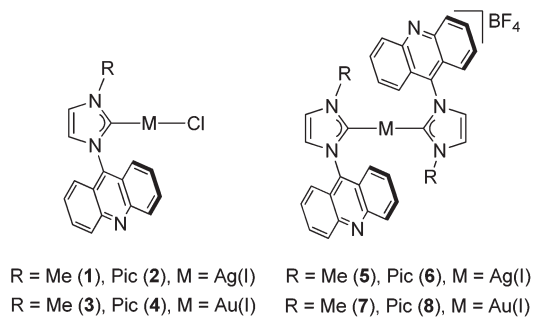

Fig. 2 Acridine wingtip N-heterocyclic complexes of Ag(I) and Au(I).

Results and discussion

Synthesis and structural characterization

The thiolate derivatives **9–12** were synthesised from the corresponding [AuCl(NHC)] precursor and mercaptopyridine or 2,3,4,6-tetra-*O*-acetyl-1-thio-β-D-glucopyranose in the presence of Cs_2CO_3 as shown in Scheme 1.

Complexes **9** and **10** show resonances in the ^{1}H NMR spectra for the NHC ligand and the new incorporated pyridine group is clearly identifiable by means of the two-dimensional COSY experiments. For complexes **11** and **12** characteristic signals at a high field assigned to the glucose group are also observed (see the Experimental section). In the $^{13}C\{^1H\}$ NMR spectra a low field displacement of more than 10 ppm is observed for the resonances of the carbene carbon atoms compared with the parent chloride complexes **3** and **4**. The mass spectra (ESI^+) show the molecular peaks for all the complexes.

The molecular structure of complex **10** determined by single crystal X-ray diffraction is depicted in Fig. 3. Further crystallographic data and the most relevant bond distances and angles are summarised in Tables S1 and S2.† The Au(1)–C(1) and Au(1)–S(1) bond distances of 2.003(3) and 2.2840(10) Å, respectively, are in agreement with those reported for the two examples of S–Au(I)–NHC complexes with the 2,3,4,6-tetra-*O*-

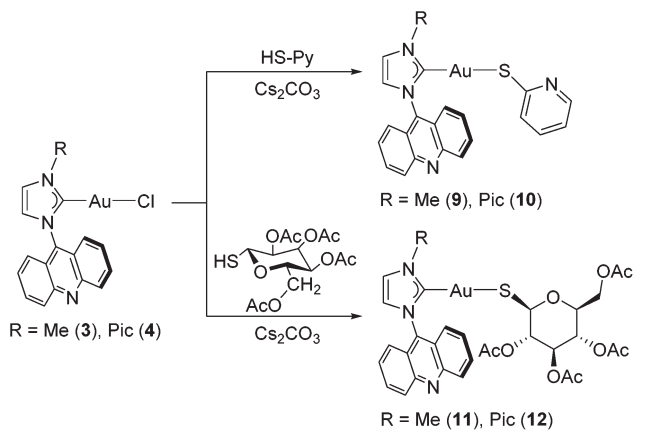

Scheme 1 Synthesis of the thiolate gold(I)–NHC derivatives.

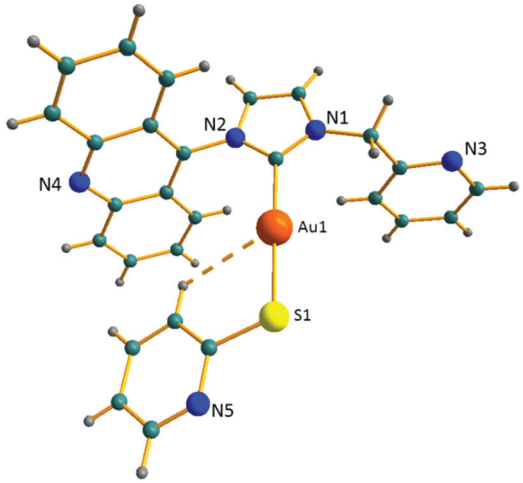

Fig. 3 Molecular structure of complex **10**.

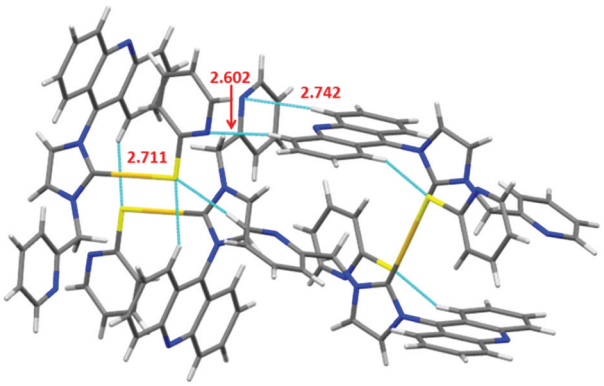

Fig. 4 Hydrogen bonds in complex **10**.

acetyl-β-D-glucopyranosyl-1-thiolato ligand, 2.04(3) and 2.28(1) for the Im^{t}Bu$_2$ and 1.986(6) and 2.2873(16) Å for the IPr (1,3-bis(2,6-diisopropylphenyl)imidazol-2-ylidene) derivatives, respectively.[19] However the Au–C$_{carbene}$ bond is slightly longer than that found in complex **3**, indicating the higher *trans* influence of the thiolate compared with the chloride ligand. The gold centre has a linear disposition with an angle C(1)–Au(1)–S(1) of 178.44(10)°, and a perpendicular disposition between the acridine and the imidazole rings is observed.

A weak intramolecular Au···H contact of 2.854 Å is observed, and several hydrogen contacts are found between the sulfur or nitrogen atoms and the protons of the acridine moiety, S1···H12 of 2.711 Å, N3···H15 2.742 Å and N5···H15 2.602 Å, forming a supramolecular structure (Fig. 4). The nitrogen atoms involved in the hydrogen bonds belong only to the pyridine moieties.

Optical properties and biological studies

The emissive properties of complexes **1–8** have been previously studied in methanol solution, showing that the emissions are acridine based with very similar energies to that of the free ligand.[17] In order to compare the luminescence properties with the biodistribution studies, the emission and excitation spectra of complexes **6**, and **10–12** were recorded in DMSO. They exhibit a structured band with emission maximum at around 484 nm for the silver bis-carbene derivative (**6**) and at *ca.* 434 nm for the thiolate complexes (**10–12**). Those emissions can be assigned to an IL transition within the acridine moiety, Fig. 5 and S1.† Moreover, despite their narrow excitation profile, with excitation maximum ranging from 407 to 427 nm, all of them can be excited at 405 nm affording emission spectra intense enough to be detected by fluorescence microscopy techniques (see section below).

The cytotoxic activity of the complexes was determined by MTT assay in two highly resistant human cancer cell lines, A549 and MiaPaca2 cells and compared to that of cisplatin. Compounds **1–12** are not soluble in water, but they are soluble in DMSO and in the DMSO/water mixtures used in the tests, which contain a small amount of DMSO. We did not observe any precipitation of the complexes or metallic gold while performing the tests. Their colourless DMSO-d_6 solutions are very stable at room temperature, as shown in the ^{1}H NMR spectra in which the signals remain the same for weeks. The results of the IC$_{50}$ values are summarised in Table 1 (final concentration < 0.5% DMSO). All the complexes showed higher cytotoxicity towards MiaPaca2 cells than towards A549 cells, see Fig. S1.† In general, Ag–NHC compounds seemed to be less cytotoxic than their Au–NHC analogs following the same trend seen by Liu, Mao and coworkers for similar Au(I) and Ag(I)–NHC complexes.[20]

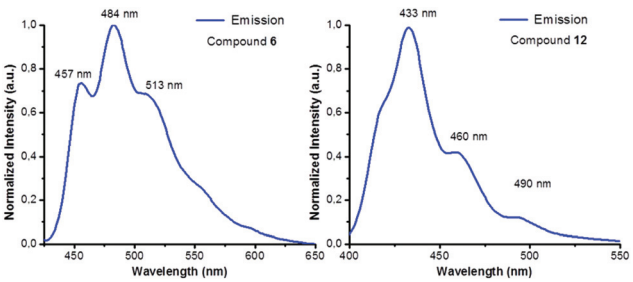

Fig. 5 Normalised emission spectra of complexes **6** and **12**.

Table 1 IC$_{50}$ (μM) of complexes **1–12** (DMSO) and cisplatin (H$_2$O)

Species	A549	MiaPaca2	Species	A549	MiaPaca2
(**1**)	>50	44.4 ± 10.9	(**8**)	41.9 ± 4.2	20.0 ± 1.6
(**2**)	>50	51.9 ± 1.9	(**9**)	>50	28.4 ± 2.5
(**3**)	>50	22.8 ± 8.8	(**10**)	17.4 ± 4.5	7.5 ± 1.2
(**4**)	>50	38.3 ± 2.6	(**11**)	19.4 ± 2.3	2.8 ± 0.8
(**5**)	>50	40.6 ± 9.9	(**12**)	13.0 ± 3.6	3.4 ± 0.8
(**6**)	>50	14.3 ± 4.3	Cis-Pt[a]	114.2 ± 9.1	76.5 ± 7.4
(**7**)	>50	6.9 ± 1.9			

[a] IC$_{50}$ value measured under the same experimental conditions as complexes **1–12**, *i.e.* incubation for 24 h at 37 °C.[21]

It is known that thiolate–Au–NHC compounds are the best mimics of the well-known auranofin, which is at the stage of clinical trials for several cancers at the moment.[22] Therefore, replacing the chloride by a thiolate derivative, and specifically by an acetylated thioglucose moiety as in auranofin, would probably lead to an increase of the cytotoxic activity.[16b,23] As predicted, the synthesised thiolate–Au–NHCs (**9–12**) turned out to be the complexes with a higher cytotoxic activity against both cell lines. In particular, complexes **11** and **12** with the tetra-*O*-acetyl-1-thio-β-D-glucopyranoside ligand have substantially smaller IC_{50} values, especially in the MiaPaca2 cells reached cytotoxicity values of 2.8 ± 0.8 and 3.4 ± 0.8 μM, respectively. As a general pattern it could be postulated that thiolate derivatives **9–12** are the most active species closely followed by the biscarbenes **5–8**, and being chloride derivatives, the species with a lower antiproliferative activity.

Since complex **12** turned out to be the most cytotoxic complex, its cell death mechanism was analysed by a flow cytometry assay. Specifically, A549 cells were incubated with complex **12** and either Annexin V-DY634 or 7-AAD as fluorescent markers. Annexin V-DY634 binds phosphatidylserine on the external surface of the cell membrane in apoptotic cells, whereas 7-AAD binds to DNA and it is efficiently excluded from intact cells, being an indicator of necrotic processes. Fig. 6 shows that Annexin V-DY634 stained a much higher percentage of cells than 7-AAD (40.6% *vs.* 16.7%), implying an apoptotic cell death pathway. Moreover, this finding was further supported with the use of Z-VAD-fmk, a cell-permeant pan caspase inhibitor. Thus, when the cells were treated with Z-VAD-fmk to induce the inhibition of caspases, *i.e.* enzymes playing essential roles in apoptotic processes, there is an evident cell death decrease for those marked with Annexin V-DY634 (40.6% *vs.* 12.3%). These data suggest a programmed cell death mechanism.

Fluorescence cell microscopy was used to ascertain cellular biodistribution of selected complexes. Their high intense emission upon excitation at 405 nm observed by fluorescence spectroscopy allowed using this excitation wavelength to visualise the new species. Thus, representative candidates from each type of complexes were chosen for the experiment in order to have a fair comparison based on their chemical structure. Specifically, A549 cells were incubated with the chloride–NHC derivative **1**, the bis-carbene species **6**, **8** and **5** and the thiolate derivatives **10**, **11** and **12** using in all cases concentrations half of their IC_{50} values, see Fig. S3–S5.† Either LysoTracker or MitoTracker, whose excitation wavelength is at 577 nm, was selected as the internal standard in order to ascertain the intracellular distribution and localization of the compounds. After 24 h of incubation, emission of all the complexes could be detected upon excitation at 405 nm, corroborating an efficient cellular uptake. Moreover, analysis of the extracellular emission intensity in row images of complexes **1** and **5**, *i.e.* the neutral chloride adduct and the corresponding cationic biscarbene, respectively, agrees with the concept that cationic species are more likely to get internalised by the cells. In addition, superimposition images with the organelle specific probes revealed a clear lysosomal localization, Fig. 7 and S4,† in contrast to the expected mitochondrial pattern for gold(I) and silver(I) compounds.[16a,20] A closer look suggests that the complexes are not only located in the lysosomes, but also seem to have some nuclear permeability and accumulation in the nucleolus. Therefore, the often-discussed antimitochondrial

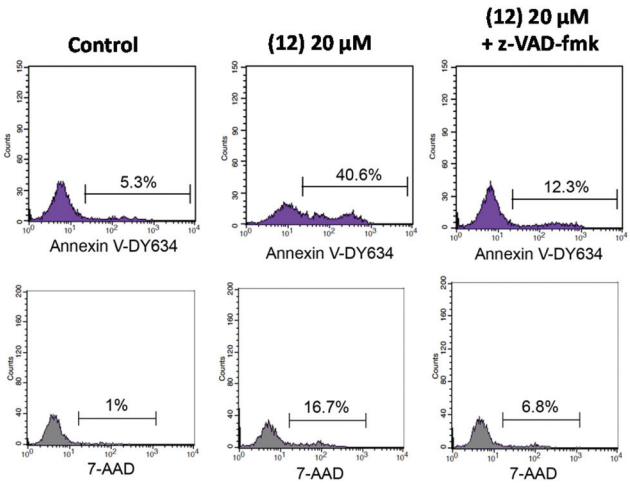

Fig. 6 Type of cell death triggered by complex **12** analysed by annexin V-DY634 and 7-ADD staining and flow cytometry.

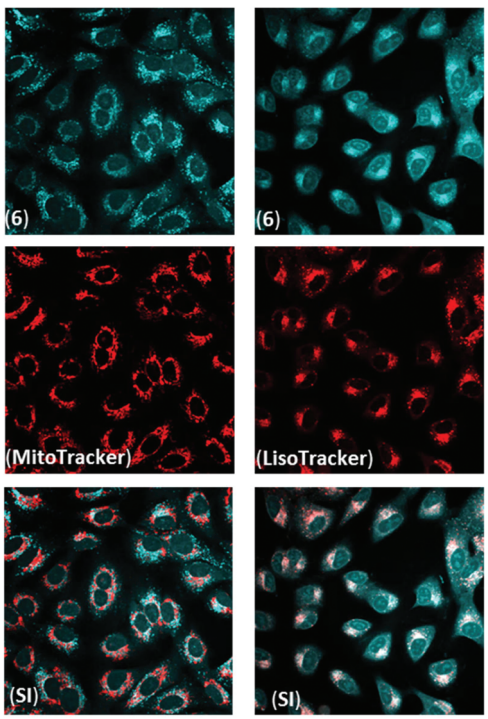

Fig. 7 Images of A549 cells incubated with complex **6** and MitoTracker (left column), **6** and LysoTracker (right column) **6** for 24 h (*C* = 1/2 of IC_{50}). Excitation at 405: emission from **6** (blue emission) and at 577 nm: emission from either the LysoTracker or MitoTracker (red emission). SI: superimposition image of complex and internal standard.

activity for gold compounds is ruled out in the present case. Instead, lysosomal accumulation was observed. Such localisation has already been reported for some dinuclear gold(I)–NHC carbenes by Baker and Berners-Price in 2006 [24] as well as for the antiarthritic gold(I) thiomalate (Myocrisin)[25] suggesting an endocytic pathway as the internalisation process as a plausible explanation. In this manner, the complexes would remain trapped in the endocytic vesicles until they finally evolve to lysosomes. However, further experiments are needed for the confirmation of this hypothesis.

Nuclear and nucleolar accumulation might be related to the affinity of Au(I) and Ag(I) to inhibit the TrxR1 and Trx1. Both enzymes are also present in the nuclear region specially in those stages of cellular stress promoted by the presence of a stress-inducing drug.[26] Previous examples reported by Mohr, Casini, Rigobello and Mao have showed nuclear accumulation for Ag(I) and Au(I)–NHC complexes.[14,16b,20] In addition to TrxR1 and Trx1 as potential biological targets, the zinc-finger enzyme PARP-1, a nuclear protein involved in DNA repair, is also known to be a target for Au(I) complexes.[27] Gold ions are able to substitute zinc ions in the PARP-1 domain of transcription.[28] On top of that, bis-carbene species could be targeting the G-quadruplex DNA by intercalation as Picquet and Casini have recently demonstrated.[29] However, if this is the case with the complexes reported here, not only are the bis-carbene species targeting the G-quadruplex DNA but also the neutral species, as all of them show the same behavior. As previously mentioned, an additional hypothesis for the nuclear and nucleolar staining that cannot be discarded is that acridine derivatives are known to be good DNA intercalators.[30] Therefore, the introduction of the acridine moiety into the NHC backbone apart from providing optimal luminescence properties, could also be delivering an additional mode of action. In fact, Ott and coworkers have already reported a similar strategy to obtain a novel Au–NHC carbene functionalised with a naphthalimide bearing a dual intracellular behaviour, both TrxR inhibition and DNA intercalation.[31] In order to shed some light on the cause of nuclear and nucleolar localisation seen in the present case, preliminary DNA interaction studies were performed for **1** and **12**, see Fig. 8. Both of them were chosen as representative complexes of neutral Ag(I) and Au(I) complexes respectively. They were incubated on plasmid (pEYFP) and the resulting changes in the electrophoretic mobility suggest that the most cytotoxic species, complex **12**, possessed some interaction character with DNA, however, complex **1** did not. This finding discards the idea that the acridine moiety might have been acting as the driving force for the nuclear staining. Therefore, the metal–NHC fragment seems to be the source for observed nuclear affinity.

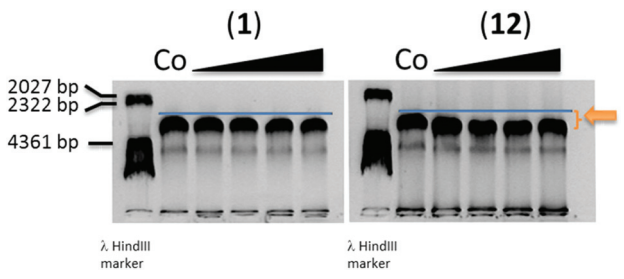

Fig. 8 Electrophoresis mobility shift assays for compounds **1** and **12**. λ HindIII: molecular weight marker; Co: control; ◀: increasing concentration of complexes; 20 μg ml^{-1} DNA, 0.4–1–2–3 metal complex: DNA bp.

Experimental section

Instrumentation

C, H, and N analyses were carried out with a PERKIN-ELMER 2400 microanalyzer. Mass spectra were recorded on a BRUKER ESQUIRE 3000 PLUS, with the electrospray ionization (ESI) technique. ^{1}H and ^{13}C{H} NMR, including 2D experiments, were recorded at room temperature on a BRUKER AVANCE 400 spectrometer (^{1}H, 400 MHz, ^{13}C, 100.6 MHz) or on a BRUKER AVANCE II 300 spectrometer (^{1}H, 300 MHz, ^{13}C, 75.5 MHz), with chemical shifts (δ, ppm) reported relative to the solvent peaks of the deuterated solvent.[32] Steady-state photoluminescence spectra were recorded with a Jobin-Yvon-Horiba fluorolog FL-3-11 spectrometer using band pathways of 3 nm for both excitation and emission.

Starting materials

The starting materials [MCl(NHC)] and [M(NHC)$_2$]BF$_4$ were prepared according to published procedures.[17] All other reagents were commercially available. Solvents were used as received without purification or drying.

General procedure for the synthesis of complexes 9–12

An excess of Cs_2CO_3 (1.5 mmol) was added to a solution of the corresponding [AuCl(NHC)] (0.1 mmol) and 2-mercaptopyridine (0.11 mmol) or thio-β-D-glucose tetraacetate (0.11 mmol) in dichloromethane. After 2 h, the reaction mixture was filtered over Celite and then concentrated under reduced pressure. The addition of hexane (*ca.* 20 ml) afforded yellow solids.

[Au(SPy)(IAMe)] (9). Yield: 0.0458 g (81%). ^{1}H NMR (DMSO-d$_6$, 300 MHz, 294 K): δ 8.35 (d, J_{H-H} = 8.6 Hz, 2H, Acr), 8.02–7.96 (m, 4H, Acr), 7.80–7.74 (m, 2H, Im, 1H, SPy), 7.62 (d, J_{H-H} = 8.4 Hz, 2H, Acr), 6.76 (t, J_{H-H} = 6.5 Hz, 1H, SPy), 6.62 (m, 1H, SPy), 6.00 (d, J_{H-H} = 7.5 Hz, 1H, SPy), 4.05 (s, 3H, CH$_3$). ^{13}C{^{1}H} NMR (DMSO-d$_6$, 75 MHz, 294 K) δ 182.9 (C$_{carb}$), 167.3 (SPy), 148.8 (Acr), 148.2 (SPy), 139.9 (Acr), 134.0 (SPy), 131.2 (Acr), 129.3 (Acr), 128.2 (Acr), 125.4 (SPy), 124.5 (Im), 123.8 (Im), 122.8 (Acr), 122.6 (Acr), 117.0 (SPy), 37.8 (CH$_3$). ESI^{+}-MS, *m*/*z*: 566.9 [M + H]$^{+}$. Anal. Calcd (%) for $C_{22}H_{17}N_4AuS$: C, 46.65; H, 3.03; N, 9.89. Found: C, 46.42; H, 3.12; N, 9.53.

[Au(SPy)(IAPic)] (10). Yield: 0.0486 g (76%). ^{1}H NMR (DMSO-d$_6$, 400 MHz, 294 K): δ 8.72–8.70 (m, 1H, Pic), 8.36 (d, J_{H-H} = 8.8 Hz, 2H, Acr), 8.11 (d, J_{H-H} = 2.0 Hz, 1H, Im), 8.02 (d, J_{H-H} = 2.0 Hz, 1H, Im), 8.00–7.96 (m, 2H, Acr), 7.92 (td, J_{H-H} = 7.7, 1.8 Hz, 1H, Pic), 7.82–7.80 (m, 1H, SPy), 7.79–7.76 (m, 2H, Acr), 7.71–7.69 (m, 2H, Acr), 7.64 (d, J_{H-H} = 7.8 Hz, 1H, Pic),

7.45–7.41 (m, 1H, Pic), 6.82–6.78 (m, 1H, SPy), 6.60–6.57 (m, 1H, SPy), 6.24–6.21 (m, 1H, SPy), 5.88 (s, 2H, CH_2). $^{13}C\{^1H\}$ NMR (DMSO-d_6, 101 MHz, 294 K) δ 184.8 (C_{carb}), 168.2 (SPy), 155.7 (Pic), 149.7 (SPy), 149.2 (Acr), 148.0 (Pic), 140.0 (Acr), 137.3 (Pic), 133.8 (SPy), 131.0 (Acr), 129.6 (Acr), 128.1 (Acr), 125.7 (SPy), 124.6 (Im), 123.6 (Im), 123.2 (Pic), 122.9 (Acr), 122.8 (Acr), 122.0 (Pic), 116.7 (SPy), 55.6 (CH_2). ESI^+-MS, m/z: 643.9 $[M]^+$. Anal. Calcd (%) for $C_{27}H_{20}N_5AuS$: C, 50.39; H, 3.13; N, 10.88. Found: C, 50.12; H, 3.02; N, 10.43.

[Au(S-D-Gluc)(IAMe)] (11). Yield: 0.0708 g (86%). ^1H NMR (acetone-d_6, 400 MHz, 294 K): δ 8.34–8.31 (m, 2H, Acr), 7.98–7.93 (m, 2H, Acr), 7.91 (d, J_{H-H} = 1.8 Hz, 1H, Im), 7.79 (d, J_{H-H} = 1.8 Hz, 1H, Im), 7.75–7.64 (m, 4H, Acr), 4.89 (t, J_{H-H} = 9.4 Hz, 1H, CH, glucose), 4.73 (t, J_{H-H} = 9.7 Hz, 1H, CH, glucose), 4.50 (d, J_{H-H} = 9.6 Hz, 1H, CH, glucose), 4.39 (t, J_{H-H} = 9.3 Hz, 1H, CH, glucose), 4.16 (s, 3H, CH_3), 3.91–3.78 (m, 2H, CH_2–OAc), 3.45 (b, 1H, CH, glucose), 1.99 (s, 3H, CH_3, OAc), 1.97 (s, 3H, CH_3, OAc), 1.93 (s, 3H, CH_3, OAc), 1.74 (s, 3H, CH_3, OAc). $^{13}C\{^1H\}$ NMR (acetone-d_6, 101 MHz, 294 K) δ 184.9 (C_{carb}), 170.7 (C═O), 170.2 (C═O), 170.1 (C═O), 169.3 (C═O), 150.4 (Acr), 131.7 (Acr), 130.8 (Acr), 128.8 (Acr), 125.0 (Im), 124.3 (Im), 123.9 (Acr), 123.8 (Acr), 83.3 (glucose), 77.8 (glucose), 76.1 (glucose), 74.8 (glucose), 70.0 (glucose), 63.7 (glucose), 38.6 (CH_3), 21.0 (CH_3, OAc), 20.7 (CH_3, OAc), 20.7 (CH_3, OAc). ESI^+-MS, m/z: 820.0 $[M]^+$. Anal. Calcd (%) for $C_{31}H_{32}O_9N_3AuS$: C, 45.43; H, 3.94; N, 5.13. Found: C, 45.72; H, 3.53; N, 4.94.

[Au(S-D-Gluc)(IAPic)] (12). Yield: 0.0750 g (84%). ^1H NMR (acetone-d_6, 300 MHz, 294 K): δ 8.71–8.70 (m, 1H, Pic), 8.34–8.30 (m, 2H, Acr), 8.02 (d, J_{H-H} = 1.9 Hz, 1H, Im), 7.98–7.92 (m, 3H, Acr, 1H, Pic), 7.83 (d, J_{H-H} = 1.9 Hz, 1H, Im), 7.75–7.67 (m, 4H, Acr, 1H, Pic), 7.44–7.40 (m, 1H, Pic), 5.90 (AB system, J_{H-H} = 15.3 Hz, CH_2, Pic), 4.90 (t, J_{H-H} = 9.3 Hz, 1H, CH, glucose), 4.71 (t, J_{H-H} = 9.7 Hz, 1H, CH, glucose), 4.53 (d, J_{H-H} = 9.5 Hz, 1H, CH, glucose), 4.44 (t, J_{H-H} = 9.3 Hz, 1H, CH, glucose), 3.91–3.77 (m, 2H, CH_2–OAc), 3.49–3.44 (m, 1H, CH, glucose), 1.98 (s, 3H, CH_3, OAc), 1.93 (s, 6H, CH_3, OAc), 1.73 (s, 3H, CH_3, OAc). $^{13}C\{^1H\}$ NMR (acetone-d_6, 75 MHz, 294 K) δ 182.5 (C_{carb}), 170.7 (C═O), 170.2 (C═O), 170.1 (C═O), 169.4 (C═O), 150.7 (Py), 150.4 (Acr), 138.3 (Pic), 131.8 (Acr), 131.7 (Pic), 130.8 (Acr), 128.9 (Pic), 128.8 (Pic), 125.2 (Im), 124.9 (Im), 124.2 (Acr), 123.9 (Acr), 123.7 (Acr), 83.4 (glucose), 78.0 (glucose), 76.1 (glucose), 74.8 (glucose), 70.0 (glucose), 63.7 (glucose), 56.7 (CH_2, Pic), 21.0 (CH_3, OAc), 20.7 (CH_3, OAc), 20.7 (CH_3, OAc). ESI^+-MS, m/z: 897.1 $[M]^+$. Anal. Calcd (%) for $C_{36}H_{35}O_9N_4AuS$: C, 48.22; H, 3.93; N, 6.25. Found: C, 47.92; H, 3.84; N, 5.89.

Crystallography

Crystals were mounted in inert oil on glass fibers and transferred to the cold gas stream of an Xcalibur Oxford Diffraction diffractometer equipped with a low-temperature attachment. Data were collected using monochromated Mo Kα radiation (λ = 0.71073 Å). Scan type ω. Absorption corrections based on multiple scans were applied using spherical harmonics implemented in the SCALE3 ABSPACK[33] scaling algorithm. The structures were solved by direct methods and refined on F^2 using the program SHELXL-97.[34] All non-hydrogen atoms were refined anisotropically. In all cases, hydrogen atoms were included in calculated positions and refined using a riding model. Refinements were carried out by full-matrix least-squares on F^2 for all data. Further details of the data collection and refinement are given in the ESI.†

DNA interaction assay

First, 10 μl aliquots of pBR322 plasmid DNA (20 μg ml^{-1}) in buffer Tris-acetate/EDTA buffer (TAE) were incubated with different concentrations of the compounds **1** and **12** (in the range 0.4–3 metal complex: DNA bp) at 37 °C for 4 h in the dark. Samples of free DNA were prepared as controls. After the incubation period, the samples were loaded onto 0.8% agarose gel containing SyBr-SAFE stain. The samples were separated by electrophoresis for 1 h at 80 V in Tris-acetate/EDTA buffer (TAE). Afterwards, the gel was visualised in a GelDoc (BioRad).

Flow cytometry assay

Cell death was analysed by measuring exposure to phosphatidylserine and membrane permeabilisation. The cells were treated for 24 h with compounds **12** at 20 μM. Then, they were trypsinised and incubated at 37 °C for 15 minutes in ABB (140 mM NaCl, 2.5 mM $CaCl_2$, 10 mM Hepes/NaOH, pH 7.4) containing 0.5 mg ml^{-1} of either annexin V-DY634 or 7-AAD. Finally, the cells were diluted to 0.5 ml with ABB and analysed by flow cytometry (FACScan, BD Biosciences, Spain).

Cell culture

HeLa (cervical cancer) and A549 (lung carcinoma) cells were maintained in high glucose DMEM (Dulbecco's Modified Eagle's Medium) supplemented with 5% fetal bovine serum (FBS), 200 U ml^{-1} penicillin, 100 μg ml^{-1} streptomycin and 2 mM L-glutamine. Cultures were maintained under a humidified atmosphere of 95% air/5% CO_2 at 37 °C. Adherent cells were allowed to attach for 24 h prior to addition of compounds.

Cytotoxicity assay

The MTT assay was used to determine cell viability as an indicator for cell sensitivity to the complexes. Exponentially growing cells were detached from the plastic flask using trypsin-EDTA solution and seeded at a density of approximately 10^4 cells per well in 96-well flat-bottomed microplates and allowed to attach for 24 h prior to addition of compounds. The complexes were dissolved in DMSO and added to cells in concentrations ranging from 0.1 to 100 μM in quadruplicate. The cells were incubated with our compounds for 24 h at 37 °C. 10 μl of MTT (5 mg ml^{-1}) were added to each well and the plates were incubated for 2 h at 37 °C. Finally, the plates were centrifuged for 10 min at 500*g*, media were eliminated and DMSO (100 ml per well) was added to dissolve the formazan precipitates. The optical density was measured at 550 nm using a 96-well multiscanner autoreader (ELISA). The IC_{50} was calculated by nonlinear regression analysis using Prism

software (GraphPad Software Inc). Each compound was analysed at least in three independent experiments.

Cell fluorescence microscopy study

European Collection of Cell Cultures were maintained in high glucose DMEM (Dulbecco's Modified Eagle's Medium) supplemented with 5% fetal bovine serum (FBS), 200 U ml^{-1} penicillin, 100 μg ml^{-1} streptomycin and 2 mM L-glutamine. The cells were detached from the plastic flask using trypsin-EDTA solution and suspended in an excess volume of growth medium. The homogeneous cell suspension was then distributed into 30 μl aliquots in a 6 channel μ-slide $IV^{0.4}$ (IBIDI), with each aliquot being subjected to incubation with the different complexes, final concentrations $\frac{1}{2}(IC_{50})$, at 37 °C for 24 h. Then, 30 μl of a solution of the internal standard, either LysoTracker Red DND-99 ($1/10^5$ dilution) or MitoTracker Red CMXRos (1/5000 dilution) in cell growth medium was added to each well. Preparations were viewed using an Olympus FV10-i Oil type compact confocal laser microscope using a ×10 or ×60 objective, with excitation wavelengths at 405 and 577 nm.

Conclusions

In conclusion, the antiproliferative activity of the acridine-based Au and Ag–NHC complexes was tested against two highly resistant cancer cells, A549 and MiaPaca2. Overall, the lung and pancreatic cells were more sensitive to the gold(I)–NHC complexes than to the silver(I)-derivatives. Moreover, cytotoxic activity for the Au–NHC complexes seems to follow a specific trend: chlorides < biscarbenes < thiolates, reaching values of $IC_{50} = 2.8 \pm 0.8$ and 3.4 ± 0.8 μM when the coordinated ancillary ligand is a tetra-*O*-acetyl-1-thio-β-D-glucopyranoside, in complexes **11** and **12** respectively. Flow cytometry and caspase-inhibition experiments showed that apoptosis was the main cell death pathway. Moreover, fluorescence cell microscopy revealed their defined biodistribution pattern, and contrary to what was expected, the complexes were mainly localised in the lysosomes and showed some nuclear and nucleolar staining. Electrophoresis analysis pointed towards the metal fragment and not the acridine moiety, as the possible source of DNA interaction, which opens the door to new and more complex mechanisms of action for Au(I) and Ag(I)–NHC complexes. This work demonstrated that it is necessary to reconsider the general hypothesis for Au(I) and Ag(I) targeting mitochondria because of their great affinity to inhibit the mitochondrial TrxR. A deeper insight is needed to eventually elucidate the biological role played by these types of Au(I) and Ag(I) complexes. Therefore, combining fluorescence microscopy techniques and optimal fluorescent bioprobes, would surely help to understand their biological interplay.

Acknowledgements

Authors thank the Ministerio de Economía y Competitividad (MINECO-FEDER CTQ2013-48635-C2-1-P, CTQ2015-70371-REDT and SAF2013-48626-C2-2-R) and Gobierno de Aragón-Fondo Social Europeo (E77) for financial support.

Notes and references

1 (*a*) N. P. E. Barry and P. J. Sadler, *Chem. Commun.*, 2013, **49**, 5016; (*b*) K. D. Mjos and C. Orvig, *Chem. Rev.*, 2014, **114**, 4540; (*c*) C. Santini, M. Pellei, V. Gandin, M. Porchia, F. Tisato and C. Marzano, *Chem. Rev.*, 2014, **114**, 815; (*d*) B. Bertrand and A. Casini, *Dalton Trans.*, 2014, **43**, 4209.

2 (*a*) S. Dasari and P. B. Tchounwou, *Eur. J. Pharmacol.*, 2014, **740**, 364; (*b*) T. C. Johnstone, K. Suntharalingam and S. J. Lippard, *Chem. Rev.*, 2016, **116**, 3436.

3 D. T. Felson, J. J. Anderson and R. F. Meenan, *Arthritis Rheum.*, 1990, **33**, 1449.

4 (*a*) C. Fan, W. Zheng, X. Fu, X. Li, Y.-S. Wong and T. Chen, *Cell Death Dis.*, 2014, **5**, e1191; (*b*) T. Zou, C. T. Lum, C.-N. Lok, J.-J. Zhanga and C.-M. Che, *Chem. Soc. Rev.*, 2015, **44**, 8786; (*c*) B. K. Rana, A. Nandy, V. Bertolasi, C. W. Bielawski, K. D. Saha and J. Dinda, *Organometallics*, 2014, **33**, 2544; (*d*) F. Cisnetti and A. Gautier, *Angew. Chem., Int. Ed.*, 2013, **52**, 11976; (*e*) W. Liu, K. Bensdorf, M. Proetto, U. Abram, A. Hagenbach and R. Gust, *J. Med. Chem.*, 2011, **54**, 8605.

5 (*a*) S. Gromer, L. D. Arscott, C. H. Williams, R. H. Schirmer and K. Becker, *J. Biol. Chem.*, 1998, **273**, 20096; (*b*) S. Urig, K. Fritz-Wolf, R. Réau, C. Herold-Mende, K. Tóth, E. Davioud-Charvet and K. Becker, *Angew. Chem., Int. Ed.*, 2006, **45**, 1881; (*c*) I. Ott, *Coord. Chem. Rev.*, 2009, 1670; (*d*) S. Nobili, E. Mini, I. Landini, C. Gabbiani, A. Casini and L. Messori, *Med. Chem. Rev.*, 2010, **30**, 550.

6 (*a*) S. Gromer, S. Urig and K. Becker, *Med. Res. Rev.*, 2004, **24**, 40; (*b*) K. Becker, S. Gromer, R. H. Schirmer and S. Müller, *Eur. J. Biochem.*, 2000, **267**, 6118; (*c*) K. Anestål and E. S. J. Arnér, *J. Biol. Chem.*, 2003, **278**, 15966.

7 C. Santini, M. Pellei, G. Papini, B. Morresi, R. Galassi, S. Ricci, F. Tisato, M. Porchia, M. P. Rigobello, V. Gandin and C. Marzano, *J. Inorg. Biochem.*, 2011, **105**, 232.

8 (*a*) W. Liua and R. Gust, *Chem. Soc. Rev.*, 2013, **42**, 755; (*b*) S. B. Aher, P. N. Muskawar, K. Thenmozhi and P. R. Bhagat, *Eur. J. Med. Chem.*, 2014, **81**, 408; (*c*) F. Hackenberg and M. Tacke, *Dalton Trans.*, 2014, **43**, 8144.

9 S. Díez-González, N. Marion and S. P. Nolan, *Chem. Rev.*, 2009, **109**, 3612.

10 R. Visbal and M. C. Gimeno, *Chem. Soc. Rev.*, 2014, **43**, 3551.

11 K. M. Lee, C. K. Lee and I. J. B. Lin, *Angew. Chem., Int. Ed. Engl.*, 1997, **36**, 1850.

12 K. Oisaki, Q. Li, H. Furukawa, A. U. Czaja and O. M. A. Yaghi, *J. Am. Chem. Soc.*, 2010, **132**, 9262.

13 (*a*) L. Mercs and M. Albrecht, *Chem. Soc. Rev.*, 2010, **39**, 1903; (*b*) L. Oehninger, R. Rubbiani and I. Ott, *Dalton Trans.*, 2013, **42**, 3269.

14 (*a*) K. M. Hindi, M. J. Panzner, C. A. Tessier, C. L. Cannon and W. J. Youngs, *Chem. Rev.*, 2009, **109**, 385; (*b*) A. Citta, E. Schuh, F. Mohr, A. Folda, M. L. Massimino, A. Bindoli, A. Casini and M. P. Rigobello, *Metallomics*, 2013, **5**, 1006.

15 C. Hemmert and H. Gorznitzka, *Dalton Trans.*, 2016, **45**, 440.

16 (*a*) L. Eloy, A.-S. Jarrousse, M.-L. Teyssot, A. Gautier, L. Morel, C. Jolivalt, T. Cresteil and S. Roland, *ChemMedChem*, 2012, **7**, 805; (*b*) B. Bertrand, A. de Almeida, E. P. M. van der Burgt, M. Picquet, A. Citta, A. Folda, M. P. Rigobello, P. Le Gendre, E. Bodio and A. Casini, *Eur. J. Inorg. Chem.*, 2014, 4532; (*c*) H. Ibrahim, C. Gibard, C. Hesling, R. Guillot, L. Morel, A. Gautier and F. Cisnetti, *Dalton Trans.*, 2014, **43**, 6989.

17 M. C. Gimeno, A. Laguna and R. Visbal, *Organometallics*, 2012, **31**, 7146.

18 L. Janovec, M. Kožurková, D. Sabolová, J. Ungvarský, H. Paulíková, J. Plšíková, Z. Vantová and J. Imrich, *Bioorg. Med. Chem.*, 2011, **19**, 1790.

19 (*a*) M. V. Baker, P. J. Barnard, S. J. Berners-Price, S. K. Brayshaw, J. L. Hickey, B. W. Skelton and A. H. White, *J. Organomet. Chem.*, 2015, **690**, 5625; (*b*) P. de Frémont, E. D. Stevens, M. D. Eelman, D. E. Fogg and S. P. Nolan, *Organometallics*, 2006, **25**, 5824.

20 Y. Li, G.-F. Liu, C.-P. Tan, L.-N. Ji and Z.-W. Mao, *Metallomics*, 2014, **6**, 1460.

21 M. Frik, J. Fernández-Gallardo, O. Gonzalo, V. Mangas-Sanjuan, M. González-Álvarez, A. Serrano del Valle, C. Hu, I. González-Álvarez, M. Bermejo, I. Marzo and M. Contel, *J. Med. Chem.*, 2015, **58**, 5825.

22 (*a*) W. Fiskus, N. Saba, M. Shen, M. Ghias, J. Liu, S. D. Gupta, L. R. Chauhan, S. Gunewardena, K. Schorno, C. P. Austin, K. Maddocks, J. Byrd, A. Melnick, P. Huang, A. Wiestner and K. N. Bhalla, *Cancer Res.*, 2014, **74**, 2520; (*b*) I. S. Kim, J. Y. Jin, I. H. Lee and S. J. Park, *Br. J. Pharmacol.*, 2004, **142**, 749; (*c*) Examples of clinical trials in progress in 2014–2015. https://clinicaltrials.gov/ct2/show/NCT01747798, https://clinicaltrials.gov/ct2/show/NCT01419691, http://www.cancer.gov/clinicaltrials/search/view?cdrid=743608&version=HealthProfessional#StudyIdInfo_CD0000743608.

23 (*a*) M. Wenzel, E. Bigaeva, P. Richard, P. Le Gendre, M. Picquet, A. Casini and E. Bodio, *J. Inorg. Biochem.*, 2014, **141**, 10; (*b*) E. Vergara, E. Cerrada, C. Clavel, A. Casini and M. Laguna, *Dalton Trans.*, 2011, **40**, 10927.

24 P. J. Barnard, L. E. Wedlock, M. V. Baker, S. J. Berners-Price, D. A. Joyce, B. W. Skelton and J. H. Steer, *Angew. Chem., Int. Ed.*, 2006, **45**, 5966.

25 J. Aaseth, M. Haugen and M. Førre, *Analyst*, 1998, **123**, 3.

26 I. Issaeva, A. A. Cohen, E. Eden, C. Cohen-Saidon, T. Danon, L. Cohen and U. Alon, *PLoS One*, 2010, **5**, e13524.

27 (*a*) F. Mendes, M. Groessl, A. A. Nazarov, Y. O. Tsybin, G. Sava, I. Santos, P. J. Dyson and A. Casini, *J. Med. Chem.*, 2011, **54**, 2196; (*b*) M. Serratrice, F. Edafe, F. Mendes, R. Scopelliti, S. M. Zakeeruddin, M. Gratzel, I. Santos, M. A. Cinellu and A. Casini, *Dalton Trans.*, 2012, **41**, 3287.

28 M. A. Franzman and A. M. Barrios, *Inorg. Chem*, 2008, **47**, 3928.

29 B. Bertrand, L. Stefan, M. Pirrotta, D. Monchaud, E. Bodio, P. Richard, P. Le Gendre, E. Warmerdam, M. H. de Jager, G. M. M. Groothuis, M. Picquet and A. Casini, *Inorg. Chem.*, 2014, **53**, 2296.

30 S. Nafisi, A. A. Saboury, N. Keramat, J.-F. Neault and H.-A. Tajmir-Riahi, *J. Mol. Struct.*, 2007, **827**, 35.

31 A. Meyer, L. Oehninger, Y. Geldmacher, H. Alborzinia, S. Wölfl, W. S. Sheldrick and I. Ott, *ChemMedChem*, 2014, **9**, 1794.

32 R. Fulmer, A. J. M. Miller, N. H. Sherden, H. E. Gottlieb, A. Nudelman, B. M. Stoltz, J. E. Bercaw and K. I. Goldberg, *Organometallics*, 2010, **29**, 2176.

33 *CysAlisPro, Version 1.171.35.11; Agilent Technologies. Multiscan absorption correction with SCALE3 ABSPACK scaling algorithm*.

34 G. M. Sheldrick, *SHELXL-97, Program for Crystal Structure Refinement*, University of Göttingen: Göttingen, Germany, 1997.

